Applied Radiation and Isotopes 203 (2024) 111108

Contents lists available at ScienceDirect

Applied Radiation and Isotopes

journal homepage: www.elsevier.com/locate/apradiso

Liquid scintillation efficiencies, gamma-ray emission intensities, and half-life for Gd-153

Denis E. Bergeron [a,*], Jeffrey T. Cessna [a], Ryan P. Fitzgerald [a], Gulakhshan Hamad [a,b], Lizbeth Laureano-Pérez [a], Leticia Pibida [a], Brian E. Zimmerman [a]

[a] Physical Measurement Laboratory, National Institute of Standards and Technology, Gaithersburg, MD, 20899-8462, USA
[b] Janssen Pharmaceuticals, Inc., Malvern, PA, 19355, USA

ARTICLE INFO

Keywords:
Activity standard
Intercomparison
International reference system
Electron capture
Decay scheme
Nuclear decay data
TDCR
Efficiency tracing

ABSTRACT

Gadolinium-153 was standardized for activity by live-timed anticoincidence counting and an ampoule was submitted to the international reference system (SIR). Absolute emission intensities for the main γ rays were determined with calibrated high-purity germanium (HPGe) and lithium-drifted silicon (Si(Li)) detectors. A revised decay scheme is indicated, with no probability of direct electron capture to the ^{153}Eu ground state. Triple-to-double coincidence ratio (TDCR) efficiency curves indicate that the revised decay scheme is consistent with experiment. Half-life measurements agree with a previous NIST determination and show no sensitivity to chemical environment.

1. Introduction

The response curve for the International Reference System (SIR) ionization chamber, estimated based on the Key Comparison Reference Values (KCRV), is modeled in a computer program referred to as SIRIC (Michotte et al., 2006; Cox et al., 2007). Gadolinium-153 is one of the few radionuclides for which the SIRIC code predicts a SIR response inconsistent with a KCRV. Given the overall success of the SIRIC model, the most likely explanations for the observed discrepancy are 1) erroneous activity assays comprising the KCRV, or 2) erroneous photon emission intensities being used for the SIRIC predictions.

NIST recently measured a solution of $^{153}GdCl_3$ in 1 mol/L HCl by live-timed 4πβ(LS)-γ(NaI(Tl)) anticoincidence counting (LTAC) and submitted an ampoule to the International Reference System (SIR) as part of the BIPM comparison BIPM.RI(II)–K1.Gd-153 (Michotte et al., 2021). This submission updated previous NIST submissions to the same comparison in 1989 and 1998, with an equivalent activity nearly identical to the 1989 submission. An updated KCRV was calculated that was significantly lower than the 2003 KCRV, and still significantly lower than the KCRV predicted by the SIRIC code (Table 1). The comparison report (Michotte et al., 2021) noted that the SIRIC code performs well for radionuclides with γ-ray emissions at similar energies to those of ^{153}Gd and concluded that the ^{153}Gd γ-ray emission intensities may be underestimated in the Decay Data Evaluation Project (DDEP, 2020; Bé et al., 2004), consistent with two newer data evaluations (Xiaolong, 2010; Nica, 2020).

The latest evaluation from the National Nuclear Data Center (NNDC, 2020; Nica, 2020) is strongly influenced by the absolute γ-ray emission intensities (I_γ) reported by Shearman et al. (2017), which indicates a need to revise the probability for electron capture directly to the ^{153}Eu ground state (i.e., the $\epsilon_{0,0}$ transition). A rebalanced decay scheme based on the Shearman et al. (2017) measurements is inconsistent with the previously-accepted (DDEP, 2020; Bé et al., 2004) 4 % probability for this transition ($P_{0,0} = 0.04$).

Precise knowledge of the ^{153}Gd decay scheme is important for γ-ray spectrometry calibrations and for applications in nuclear medicine. The γ-ray emissions at 97 keV and 103 keV make ^{153}Gd line sources appealing for patient-specific attenuation corrections in single photon emission tomography (SPECT) because their relatively low energies result in minimal dose to patients (Frey and Tsui, 1995; Perisinakis et al., 2002; Case, 2015). In addition, activity assays and dosimetry calculations for potential brachytherapy applications (Enger et al., 2013; Famulari et al., 2017, 2018) depend on the adopted γ-ray emission intensities.

Consistent with the Shearman et al. (2017) results, we present herein measurements from multiple methods that support a decay scheme with

* Corresponding author.
E-mail address: denis.bergeron@nist.gov (D.E. Bergeron).

https://doi.org/10.1016/j.apradiso.2023.111108
Received 31 May 2023; Received in revised form 23 October 2023; Accepted 6 November 2023
Available online 9 November 2023
0969-8043/Published by Elsevier Ltd.

Table 1
Equivalent activities (A_{ei}) and uncertainties (u_{ci}) from BIPM.RI(II)–K1.Gd-153 (Michotte et al., 2021).

	A_{ei} / MBq	u_{ci} / MBq
NIST 2020	362.1	2.2
KCRV 2003	367.7	1.7
KCRV 2020	364.2	2.0
SIRIC	383.8	6.4

$P_{0,0} = 0$. Sources with activities traceable to the LTAC calibration were measured by liquid scintillation counting, including triple-to-double coincidence ratio (TDCR) counting, providing a set of LTAC-based empirical LS efficiencies against which calculated efficiencies could be benchmarked. Calculated TDCR efficiencies are particularly sensitive to the adopted electron capture branching scheme (Broda, 2003) and the experimental data are clearly more consistent with a scheme that excludes the $\epsilon_{0,0}$ transition. Sources were also measured with calibrated high-purity germanium (HPGe) and lithium-drifted silicon (Si(Li)) detectors to determine I_γ for the main γ rays. The I_γ results were generally consistent with Shearman et al. (2017), but our use of a Si(Li) detector, with nearly linear efficiency at lower energies, allowed for an improved measurement of the 69.7 keV γ ray.

Finally, new half-life measurements were acquired over up to 3 half-lives with ionization chambers, a well-type NaI(Tl) detector, and a HPGe detector.

2. Methods and materials

2.1. Source preparation

Dilutions were prepared from a ^{153}Gd source ($GdCl_3$ in 1 mol/L HCl) received from Eckert & Ziegler Isotope Products (Valencia, CA, USA).[1] All dilutions were carried out gravimetrically using a carrier solution containing 107.5 μg/g of $GdCl_3$ in 0.48 mol/L HCl. Gravimetric dilution factors were confirmed by ionization chamber or HPGe spectrometry and no losses were observed. Serial dilutions produced a series of 5 mL flame-sealed ampoules (NIST Type 1; Collé, 2019) with massic activities ranging from 7.0 MBq/g to 22 kBq/g. The ampoule submitted to the SIR (Michotte et al., 2021) was a direct dilution of the primary solution. Ampoules measured on ionization chambers at NIST (Vinten 671, IC "A", and "AutoIC") were also direct dilutions of the primary solution with dilution factors ($f_{\mathrm{dil}} = \frac{m_a+m_c}{m_a}$, where m_a is the mass of active solution and m_c is the mass of carrier solution) of 7.3 to 9.9. The 22 kBq solution used to prepare liquid scintillation (LS) counting sources was linked to the primary solution by three dilutions with $f_{\mathrm{dil}} = 3.8$, 16.2, and 5.0. Two point sources were prepared from the first of these dilutions ($f_{\mathrm{dil}} = 3.8$) for HPGe measurements.

The LS counting sources included three custom-built glass hemispheres, prepared with Ultima Gold (UG; PerkinElmer, Wesley, MA, USA) liquid scintillator brought to a total aqueous fraction ($f_{\mathrm{aq}} = \frac{m_{\mathrm{aq}}+m_s}{m_{\mathrm{aq}}}$, where m_{aq} is the mass of aqueous solution and m_s is the mass of liquid scintillator) of 3 % with the carrier solution. A matched blank hemisphere was also prepared with the same scintillator and aqueous fraction. The hemispheres were sealed with epoxy and allowed to dark-adapt prior to measurement. Two sets of five nitromethane-quenched LS sources were prepared in polyethylene vials. One set was prepared with UG with $f_{\mathrm{aq}} = 3$ % and the second with Ultima Gold AB (UGAB; PerkinElmer, Wesley, MA, USA) with $f_{\mathrm{aq}} = 7$ %. These ten sources and matched blanks were used for both the triple-to-double coincidence ratio (TDCR) and CIEMAT-NIST efficiency tracing (CNET) methods of liquid scintillation counting. For CNET, an additional set of ten ^{3}H sources was prepared from a dilution of SRM 4927g (NIST, 2015) with compositions matching the ^{153}Gd set.

Finally, for half-life measurements using a well-type NaI(Tl) detector, two 5 mL flame-sealed ampoules were prepared with 0.3 g and 0.6 g of the 22 kBq/g ^{153}Gd solution and brought to approximately 5 mL with carrier solution. Subsequently, additional half-life sources were prepared in glass scintillation vials: two "dry" sources, in which activity was deposited onto filter paper and allowed to dry, two sources prepared in 5 mL of 1 mol/L HCl, and two sources prepared in 5 mL of concentrated (12.1 mol/L) HCl.

2.2. Live-timed 4 $\pi\beta(LS)$-$\gamma(NaI)$ anti-coincidence counting

The three hemisphere sources and a matched blank were measured on a single-PMT (photomultiplier tube) live-timed 4 $\pi\beta$(LS)-γ(NaI) anti-coincidence (LTAC) system (Lucas, 2008; Fitzgerald and Schultz, 2008). List mode data were acquired with a CAEN DT5724 digitizer (CAEN S.p. A., Viareggio, Italy) and efficiency variation was achieved in processing by varying the lower-level discriminator in the LS channel. Each source was measured once on the day selected for the reference time; the standard deviation of the distribution for the three massic activities was 0.04 %. Three days later, one of the sources was measured a second time with higher LS gain; the resulting massic activity was within 0.04 % of the first measurement.

Geant4 (Agostinelli et al., 2003) Monte Carlo simulations were run for matched experimental conditions. The specific LTAC model has been previously described (Fitzgerald, 2016; Bergeron and Fitzgerald, 2018). The default decay data used by Geant4 (v. 4.9.5) was based on the 2012 Evaluated Nuclear Structure Data File (with data from Helmer, 2006), with $P_{0,0} = 0.04$. In this work, the default data were replaced with DDEP (Bé et al., 2004) values or with values derived from Shearman et al. (2017). The input data are summarized in the online supplemental data (Table S1). In both cases, the default nuclear and atomic relaxation data were preserved.

Efficiency extrapolations were based on three anticoincidence gates in the NaI(Tl) channel: G1 was set over the x-ray region, G2 was centered on the 100 keV γ-ray region, and G3 was set over the 140 keV region that included coincident summing of multiple-photon cascades. Fig. 1 shows the gates drawn over experimental NaI(Tl) spectra; simulated spectra were nearly identical.

2.3. Liquid scintillation counting

The same set of liquid scintillation (LS) sources was used for both CNET and TDCR counting. Each of the five nitromethane-quenched UG

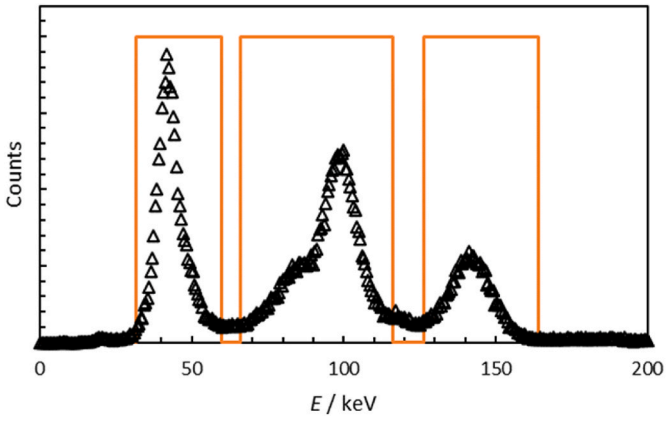

Fig. 1. Experimental NaI(Tl) spectra and LTAC gates G1, G2, G3 (left to right).

[1] Certain commercial equipment, instruments, or materials are identified in this paper to foster understanding. Such identification does not imply recommendation by the National Institute of Standards and Technology, nor does it imply that the materials or equipment identified are necessarily the best available for the purpose..

sources, along with matched blanks, were measured on the NIST TDCR counter (Zimmerman et al., 2004) four days before the reference time. Each time a source was placed into the detector, three counts with 600 s live time each were collected using a field-programmable gate array-based system with imposed extending deadtime of 50 μs and a coincidence resolving time of 150 ns, resulting in approximately 10^6 doubles counts. The three least-quenched sources were placed into the chamber two more times for a total of three insertions with three 600 s counts each. The least-quenched UGAB source was also counted. Four days later, on the day selected for the reference time, the three least-quenched UG sources were counted again with an average difference between the results of 0.03 %. At these experimental count rates, contributions from accidental coincidences (Dutsov et al., 2020) were negligible.

All of the nitromethane-quenched UG and UGAB sources, along with matched blanks and matched tritium sources, were counted on a Beckman Coulter LS6500 (Beckman Coulter, Fullerton, CA, USA) and a Packard Tri-Carb 4910 (PerkinElmer, Waltham, MA, USA). Each source was counted for 600 s per cycle with five cycles on the Beckman starting four days before the reference date, and another five cycles four days after the reference date; the same counting conditions were set for the Tri-Carb with five cycles starting ten days after the reference date and another five cycles 15 days after the reference date. The average massic activity from the first set of cycles to the second set of cycles was consistent to <0.04 %. The average massic activity determined with the Beckman was consistently higher (by approximately 0.8 %) than with the Tri-Carb.

Counting efficiencies for both TDCR and CNET were calculated using the MICELLE2 code (Kossert and Grau Carles, 2010). Initially, the DDEP (Bé et al., 2004) data were adopted and the large uncertainty associated with the branching was noted as a major source of uncertainty. The four branches were run independently and the output combined according to the branching ratios. After re-balancing the decay scheme using the Shearman et al. (2017) data, the efficiencies were re-calculated. Fig. 2 shows the LS efficiencies from the MICELLE2 model using the different decay data.

The KL1L2L3M atomic rearrangement model realized in MICELLE2 has been shown to give reasonable results for electron capture nuclides with $Z \lesssim 58$, but more atomic shells may need to be included for higher-Z (Kossert and Grau Carles, 2010).

PMT asymmetry effects were also considered. Using the mono-energetic approximation described by Kossert et al. (2020), the correction factor was determined to be $k_{\mathrm{asym}} \leq 1.00007$. Larger corrections were indicated with an implementation of the stochastic approach to asymmetry corrections also described by Kossert et al. (2020). The MICELLE2 code was modified to write electron energies E_{il} for each electron in a simulated decay event to a file, with each line recording $E_{il}Q$ (E_{il}), the event energy corrected for the energy-dependent quench function. For ^{153}Gd, the electron capture branches were weighted according to the branch probabilities by changing the number of events (i.e., the number of lines in the $E_{il}Q$ (E_{il}) log file) according to the adopted decay scheme. A numerical minimization was carried out using the ROOT framework (Brun and Rademakers, 1997), which provides a variety of minimization techniques. The "GSLMinimizer" (Moneta, 2010) was selected here, with the "kConjugatePR" algorithm. As described by Kossert et al. (2020), the minimization is designed to find the values for the three free parameters that best describe the experimental data, allowing an optimal estimation of the counting efficiencies for all three double coincidence counting channels.[2]

[2] The code developed here to correct for PMT asymmetry in TDCR counting will be made available upon request.

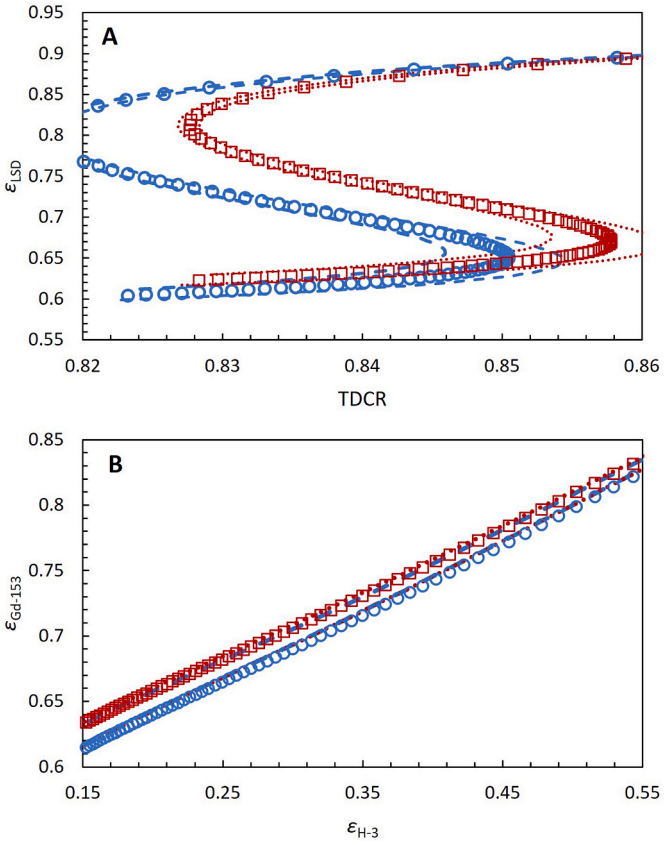

Fig. 2. Liquid scintillation efficiencies calculated for (A) TDCR and (B) CNET. The blue open circles represent calculations using the $P_{0,0} = 0.04$ branching, while the red open squares show $P_{0,0} = 0$. The curves were calculated with $kB = 0.0075(15)$ cm MeV^{-1}, where the kB uncertainty bands are shown as blue dashed ($P_{0,0} = 0.04$) or red dotted ($P_{0,0} = 0$) lines.

2.4. Vinten 671 ionization chamber

Four ampoules from the first dilution ($f_{\mathrm{dil}} = 3.8$) were measured on a Vinten 671 ionization chamber (VIC; serial number 3–2, Vinten Instruments, Surrey, UK) biased to −1500 V and read by a Keithley 6517A electrometer (Keithley Instruments, Cleveland, OH, USA). A LabVIEW (National Instruments, Austin, TX, USA) interface collected 2000 time-stamped current readings with 1.5 s between readings.

From the current measurements, a calibration coefficient, K_{VIC} (with units pA/MBq), was determined for ^{153}Gd in a 5 mL flame sealed ampoule based on the LTAC-determined activity. For comparison, values of K_{VIC} were determined with a Monte Carlo model built in EGSnrc (Kawrakow et al., 2000) using the egs_chamber application and based in part on the work of Townson et al. (2018). The development and benchmarking of the model is described in a separate contribution to these proceedings (Broder et al., 2023). The egs_radionuclide_source library was used to input decay data from evaluated nuclear structure data files (ENSDF) downloaded from the decay data evaluation project (DDEP) website. The ENSDF files were modified to simulate the rebalanced decay scheme with $P_{0,0} = 0$.

2.5. HPGe gamma-ray spectrometry

The γ-ray spectrometry measurements were performed with 5 mL flame-sealed ampoules and point sources using three different detectors: two HPGe detectors (referred to as the X-detector and the G-detector) and one Si(Li) detector (referred to as the S-detector). For the energy region of interest, the full energy peak efficiency values for the detectors were previously determined using NIST-calibrated point sources and

ampoules containing 5 mL of calibrated solutions for ^{241}Am, ^{210}Pb, ^{133}Ba, ^{109}Cd, ^{57}Co, ^{152}Eu, ^{207}Bi and ^{137}Cs that cover the energy region of interest. The photon emission intensities used for the detector calibrations were taken from DDEP. The measurement distances from the HPGe detectors varied from 20 cm to 40 cm, depending on the source activity. The measurements in the S-detector were performed at a 5 cm distance. These detectors are equipped with source holders that allow for repeatable repositioning of the source on top of the detectors. The S-detector is calibrated for use over an energy range from 14 keV to 140 keV while the HPGe detectors are calibrated for use over a range of approximately 30 keV to 1.8 MeV. The data from the HPGe detectors were analyzed using two different software packages (Genie, 2000, Mirion, Atlanta, GA, USA; FitzPeaks, JF Computing Services, Oxfordshire, UK). The data for the S-detector were analyzed using FitzPeaks only. The detectors' main characteristics are listed in Table 2.

The HPGe detectors are shielded with lead with cadmium and copper lining. The S-detector has no shielding, due to the low-energy measurement range and low background in this measurement region as well as the low detection efficiency.

The response of the HPGe detectors and the S-detector is different in the low-energy region. While the HPGe detectors show a large curvature, the Si(Li) displays almost a linear response function. Fig. 3 shows the full energy peak efficiency for the 5 mL ampoules as a function of photon energy for the S-detector at a source to detector distance of 5 cm, for the X-detector at a source to detector distance of 25 cm and for the G-detector at a source to detector distance of 20 cm.

The full energy peak efficiency for the ^{153}Gd γ rays (i.e., 69.7 keV, 97.4 keV, and 103.2 keV) measured using the S-detector point source geometry was determined using the DDEP (2011) and Shearman et al. (2017) emission intensities to look at the differences between the different published values, see Fig. 4.

A 5 mL flame sealed ampoule containing approximately 500 kBq of ^{153}Gd at the time of measurement was used to perform the impurity measurements. No γ-ray emitting impurities were detected. The detection limits for this measurement are listed in Table 3.

Emission intensity measurements were performed both in the HPGe detectors and the S-detector. The measurement time varied from 1 d to 2 d. The longer measurement times were for the S-detector due to its low detection efficiency. The measurements were performed using both point sources and 5 mL ampoules.

There are advantages and disadvantages to measuring the ^{153}Gd sources with HPGe detectors and Si(Li) detectors. The differences in the spectral shapes can be seen in Fig. S1, Fig. S2, and Fig. S3. The main considerations when comparing the spectra acquired using the two detector types are the higher efficiency for HPGe and the more linear efficiency curve and lower background for Si(Li).

2.6. Half-life measurements

2.6.1. HPGe detector

Half-life measurements were performed on one HPGe detector using a 5 mL flame-sealed ampoule with an initial ^{153}Gd activity of 450 kBq. The source was measured for 518 d with each individual measurement set for 1 d. The source-to-detector distance was set to 40 cm. Due to the long half-life, the source was occasionally removed between runs as the detector was used for other measurements. The source was repositioned in the same location for each measurement. Measurements were stopped after 518 d as the detector was moved to a new location.

The 97.4 keV γ ray was used to determine the half-life. The count rates were corrected for pile-up and decay during the measurement time.

2.6.2. Ionization chamber

Half-life measurements were performed using the Vinten 671

Table 2
Gamma-ray spectrometer main characteristics.

Variable	S-detector	X-detector	G-detector
FWHM – 69 keV	0.44 keV	0.429 keV	1.116 keV
97 keV	0.51 keV	0.487 keV	1.201 keV
103 keV	0.53 keV	0.498 keV	1.204 keV
122 keV	0.568 keV	0.525 keV	1.212 keV
Crystal diameter	10 mm	49.7 mm	58.0 mm
Crystal length	5 mm	22.1 mm	57.6 mm

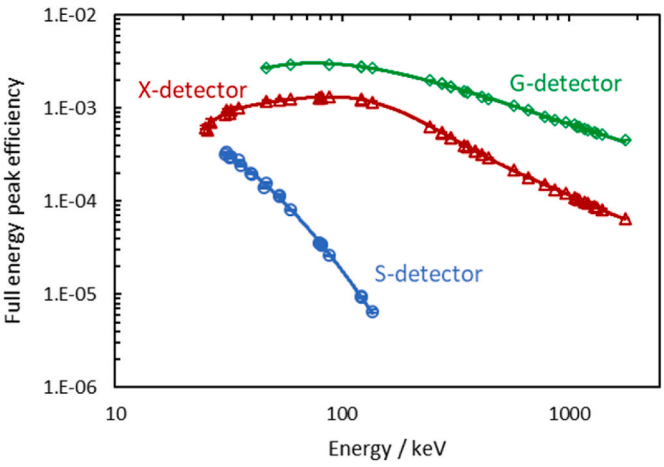

Fig. 3. Full energy peak efficiency as a function of photon energy for the 5 mL ampoules for the S-detector at a source to detector distance of 5 cm (blue circles), for the X-detector at a source to detector distance of 25 cm (red triangles) and for the G-detector at a source to detector distance of 20 cm (green diamonds). The lines are the polynomial fit to the measured data points.

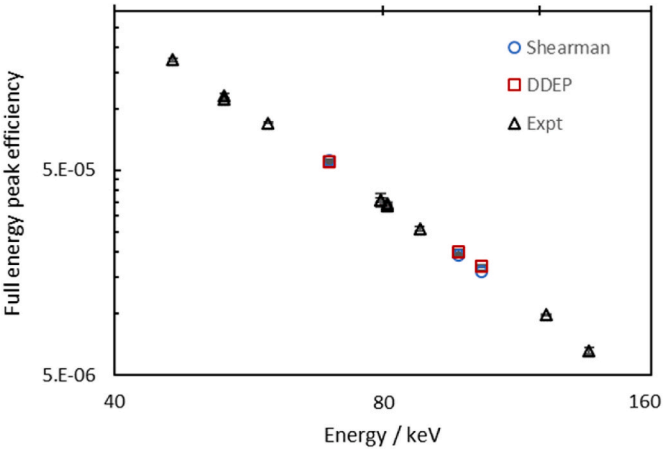

Fig. 4. Full energy peak efficiency as a function of photon energy for the S-detector using point sources at a source to detector distance of 5 cm (black triangles). ^{153}Gd points were included using the DDEP (red squares) and Shearman et al. (blue circles) emission intensities.

Table 3
Photon detection limits of ^{153}Gd source as of 10/27/2020 2:20:00 p.m. EST.

Energy range / keV	Detection limits / s^{-1}
30 to 50	380
55 to75	67
80 to 105	210
110 to 240	12
245 to 770	6.7

ionization chamber (VIC). A 5 mL flame sealed ampoule with initial ^{153}Gd activity of 13 MBq was measured using the appropriate ampoule holder. Current readings were taken with the Keithley 6517A electrometer. The LabVIEW interface was configured to collect 2000 time-stamped current readings with 1.5 s between readings and then wait 11.2 h before collecting the next set of 2000 readings so that the data acquisitions were spaced 12 h apart. Data were collected over a period of 725 d, with occasional interruptions for other measurements. All data fell within a single electrometer range, so no corrections or uncertainties associated with range changes were encountered. Periodic measurements of a ^{226}Ra reference source assured stable operation over the span of the measurements and were used to estimate the relative uncertainty associated with source placement. Each 2000-reading measurement was averaged and the standard deviation of the mean was used in the fit weighting for the half-life determination.

2.6.3. NaI(Tl) well-type detector

Half-life measurements were performed on the Wizard 2480 (PerkinElmer, Waltham, MA, USA) well-type NaI(Tl) detector with a total of eight ^{153}Gd sources: two 5 mL ampoules containing ^{153}Gd in 1 mol/L HCl and six LS vials with 2 each of ^{153}Gd in 1 mol/L HCl, concentrated HCl and deposited on filter paper. Matched blanks for each source type were also counted, along with a long-lived ^{129}I check source. The sources, blanks, and check source were counted for 2 h each and cycled for up to 840 d with rare interruptions for other measurements.

3. Results

3.1. LTAC activity

The activity determined by 4πβ(LS)-γ(NaI(Tl)) live-timed anticoincidence counting (LTAC) was the basis for the 2020 NIST submission to the SIR (Michotte et al., 2021). The data used to define the curves for extrapolation to zero inefficiency ($Y = 0$) used lower level discriminator settings in the low-energy region of the LS spectrum (Fig. 5) to avoid extrapolating over an observed discontinuity. An extended dataset was considered for the uncertainty evaluation.

The anticoincidence data for the three gates agree well with Monte Carlo simulations (Fig. 6). The data acquired with the two γ-ray gates (G2 and G3) agree better with the data simulated with $P_{0,0} = 0$. The data acquired with the x-ray gate (G1) fall between the data simulated with $P_{0,0} = 0.04$ and $P_{0,0} = 0$.

Initial Geant4 simulations were used to identify weights (a_i) that would give the true activity when extrapolating N_{LS} to $Y_{eff} = 0$ (where $Y_{eff} = a_1Y_1 + a_2Y_2 + a_3Y_3$). However, doing so led to significant trends in the fit quadratic form. Those residuals indicated an extrapolation that was not robust against the endpoints (LS efficiency range), and likely sensitive to small mismatches between the model and experiment.

Six sets of weights, $\{a_1, a_2, a_3\}$, were examined and the weights that led to the smallest residuals, minimal dependence on input data, and nearly the true activity, were {0.70, 0.28, 0.12}. Note, {0.25, 0.16, 0.15} gave almost identical results and corresponds to the NaI efficiencies for the three gates, thus roughly approximating a large, open gate.

The {0.70, 0.28, 0.12} weights with a narrow LS efficiency range (over the L x-ray region only) defining the linear fit used for extrapolation gave an intercept of $N_{LS} = 1.001$ with $P_{0,0} = 0$ and $N_{LS} = 0.999$ with $P_{0,0} = 0.04$. Thus, the simulations suggest that the s6 weights would produce correction factors for experimental intercepts of $f = 1.001$ and $f = 0.999$, respectively. In practice, no correction was made. Residuals from s6 are shown in Fig. 7.

Table 4 summarizes the statistical analysis of the experimental data for the 6 sets of weights for both wide and narrow LS efficiency ranges used in the linear fit (extrapolation to zero inefficiency), along with corresponding results that would be produced by applying corrections based on Monte Carlo simulations using input data with and without the $\epsilon_{0,0}$ transition. For both wide and narrow LS efficiency ranges, applying

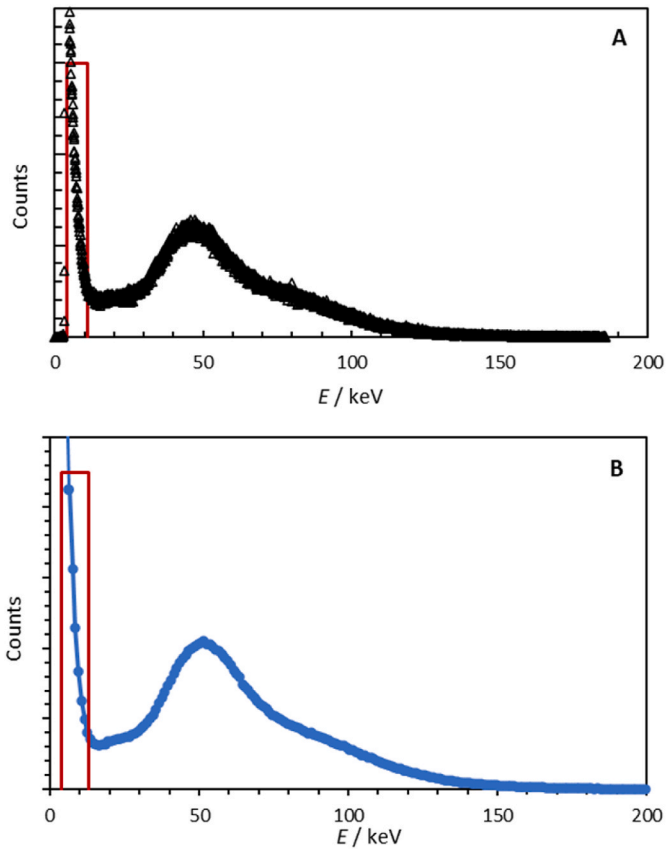

Fig. 5. (A) Experimental and (B) simulated LS spectrum. The red box shows the region over which the LLD was varied to allow extrapolation to $Y = 0$.

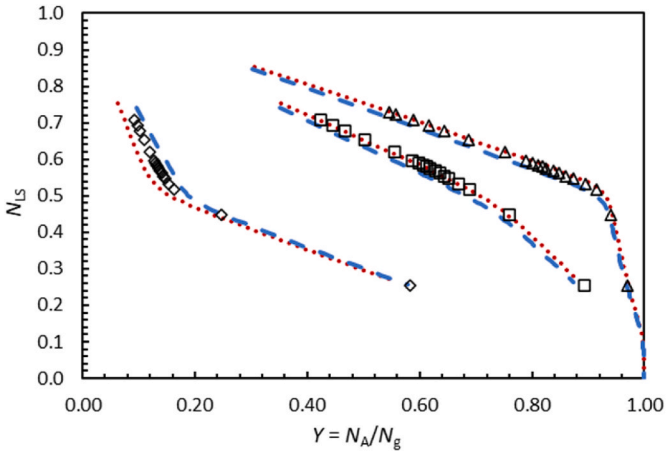

Fig. 6. Experimental LTAC data for G1 (open diamonds), G2 (open squares), and G3 (open triangles). Monte Carlo simulated data show the case with $P_{0,0} = 0.04$ (blue dashed lines) and with $P_{0,0} = 0$ (red dotted lines).

Monte Carlo corrections from either data set reduces the standard deviation by about a factor of 2.5, with the $[P_{0,0} = 0]$ data resulting in slightly lower standard deviation (but not significant). For the wide LS efficiency range, the correction based on the Monte Carlo data with $P_{0,0} = 0.04$ performs better, reducing the standard deviation by 9x as opposed to 1.5x for the $[P_{0,0} = 0]$ data. Some of the sets resulted in large trends in the extrapolation residuals, which would exclude those sets from use in an activity determination, but they are included in the uncertainty evaluation to provide a conservative estimator of the sensitivity of the measurement result to the extrapolation.

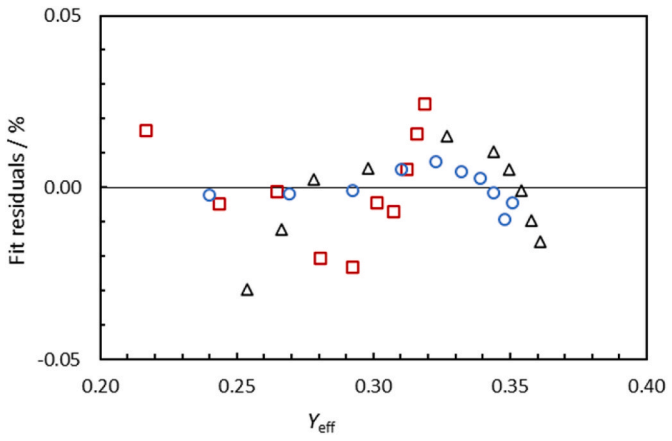

Fig. 7. Fit residuals for {0.70, 0.28, 0.12} weights over a narrow LS efficiency range one source (black open triangles), and for Monte Carlo simulations with $P_{0,0} = 0.04$ (blue open circles) and $P_{0,0} = 0$ (red open squares). There is a small trend in the experimental residuals, which is better reproduced by the simulation with $P_{0,0} = 0.04$. For some of the other sets of weights, fit residuals up to 0.4 % were observed.

Table 4
Summary statistics for extrapolations with 6 sets of weights over either narrow or wide LS efficiency ranges. Experimental results for narrow and wide ranges. Mean difference (D) from best value and standard deviation (s) among 6 sets of weights, where best value is {0.70, 0.28, 0.12}, narrow.

	uncorrected		$P_{0,0} = 0.04$		$P_{0,0} = 0$	
LS range	D / %	s / %	D / %	s / %	D / %	s / %
narrow	0.12	1.38	0.04	0.63	−0.28	0.49
wide	0.37	4.02	0.29	0.46	−0.34	2.67

The final massic activity value was taken as the arithmetic mean of the intercepts for three sources. The complete uncertainty budget for the LTAC-determined massic activity is given in Table 5. The extrapolation uncertainty is conservatively estimated from the average of the standard deviations on the Monte Carlo-corrected intercepts calculated with and without the $\epsilon_{0,0}$ transition and using the narrow LS efficiency range (Table 4).

3.2. LS efficiencies

Experimentally observed values for the triple-to-double coincidence ratio (R) ranged from approximately 0.843 to 0.855. Over this range, increased quenching resulted in increased R, allowing an unambiguous identification of the region of the efficiency curve to be considered. Using the MICELLE2 model with the DDEP input data, however, gives an efficiency curve that does not allow for the experimentally observed values of R. This is illustrated in Fig. 8A, where the data are forced onto one or the other of the efficiency curves calculated with $P_{0,0} = 0$ or $P_{0,0} = 0.04$. This forcing is achieved by calculating a massic activity for the highest efficiency data based on the MICELLE2 models and then using that massic activity with the experimental count rates and masses to generate empirical efficiencies. The data forced onto the [$P_{0,0} = 0$] model fits the curve reasonably well, with some drop off near the inflection point. The data forced onto the [$P_{0,0} = 0.04$] model follows the curve up to $R = 0.85$ and then continues on its trajectory past the model's inflection point. It has been observed that this behavior is visually reminiscent of the cartoon character who runs off the edge of a cliff without falling and so we refer to a "Wile E. Coyote region" of an efficiency curve.

Similar observations have been reported for other radionuclides with uncertain electron capture branching. In standardizing ^{64}Cu by TDCR counting, Amiot et al. noted that the calculated efficiencies did not allow the full range of experimentally observed values for R until a reevaluation of the decay scheme, with a 3 % difference on the ratio $P_{ec}/P_{\beta+/-}$ (Amiot et al., 2012). Others, too, have since discussed TDCR measurements of ^{64}Cu and the uncertainties resulting from the branching in this complex decay scheme (Kossert et al., 2014; Bergeron et al., 2018).

The dashed lines in Fig. 8B show the large uncertainties on the TDCR counting efficiencies that result from the uncertainties on the DDEP electron capture branching probabilities. Fig. 8B also shows the empirical counting efficiencies calculated from the LTAC-determined massic activity. These efficiencies, given as supplemental data in Table S3 to allow benchmarking of efficiency models, are consistent with a lower

Table 5
LTAC uncertainty budget.

Uncertainty Component	u_i / %	Comments
Sample-to-sample	0.03	SD in distribution $N = 3$
extrapolation	0.56	SD from $N = 6$ extrapolations (weights & ranges) averaged over 2 geant4 models
live-time	0.1	From previous systematic tests
masses	0.05	typical
Background	0.03	partially embodied in sample-to-sample
decay-correction	4E-05	From DDEP half-life
impurities	0	none seen
combined	**0.58**	
U_c ($k = 2$)	**1.15**	

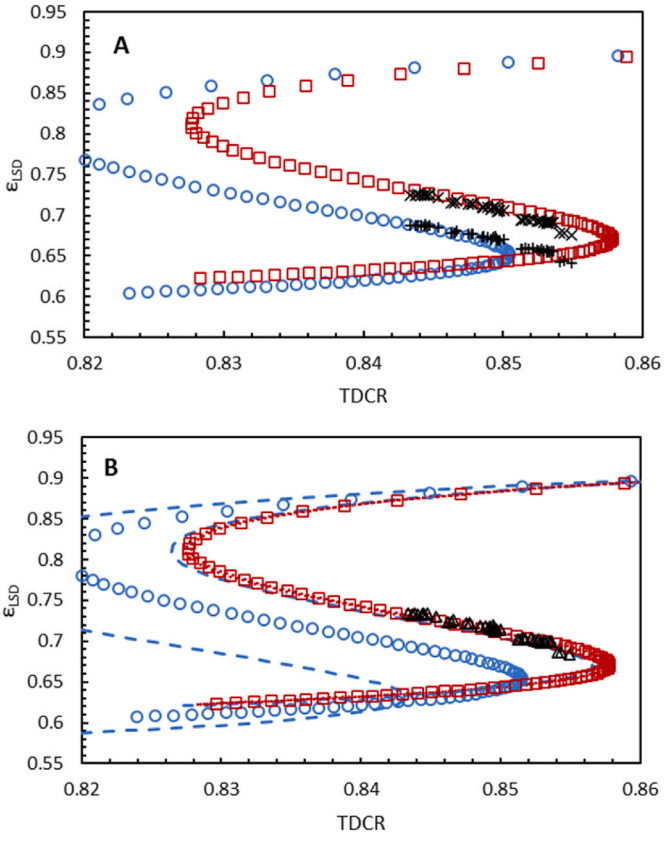

Fig. 8. (A) Efficiency curves calculated from MICELLE2 with experimental data forced onto the $P_{0,0} = 0.04$ (Xs) or $P_{0,0} = 0.04$ (+s) curves. (B) Efficiency curves calculated from MICELLE2 with empirical efficiencies (open triangles) calculated from the experimental data and LTAC-determined massic activities. The uncertainty bands represent the propagation of the DDEP uncertainty (blue dashed lines) or the uncertainty estimated from the I_γs from Shearman et al. (2017) (red dotted lines) on the electron capture branching.

value for $P_{0,0}$. Again, it should be noted that the KL1L2L3M atomic rearrangement model is thought to be insufficient for electron capture nuclides with $Z \gtrsim 58$ (Kossert and Grau Carles 2010), but the gross improvement of the model with reduced $P_{0,0}$ is at least consistent with the rebalanced decay scheme implied by Shearman et al. (2017) and this work.

The same MICELLE2 model is used to calculate efficiencies for CIEMAT-NIST efficiency tracing (CNET) with tritium (Fig. 2B). The sensitivity to the branching ratios is still present, as expected since the γ-rays from the excited states are highly converted, resulting in much higher efficiency for these branches than for the $\epsilon_{0,0}$ transition. However, without the "Wile E. Coyote region" observed in the TDCR experiment, it is impossible to detect a problem with the efficiency model. In this particular instance, CNET measurements performed in isolation (i.e., without complementary TDCR measurements) could allow a "hidden bias"—a bias that would be present, but not hidden, using the same efficiency model for TDCR.

Such a "hidden bias" also manifests in the "*K*3" solution proposed by Broda (Broda et al., 1998; Broda, 2003) as a means of avoiding "non-single-valued" TDCR efficiency curves. Broda suggested using a *K*3 parameter, defined as the ratio of a triple coincidence efficiency, ε_T, to a sum of double coincidences, ε_D to the third power

$$K3 = \frac{\varepsilon_T}{\varepsilon_D^3} = \frac{N_0^2 N_T}{N_D^3} \quad (1)$$

as a means of achieving monotonic efficiency curves for electron capture nuclides.

Using the ε_D and ε_T outputs from the MICELLE2 model, and N_D and N_T from the experiment, this approach was implemented for ^{153}Gd. For each set of nuclear data inputs or *kB*, a *K*3 efficiency curve was generated. Fig. 9 shows the *K*3 efficiency curves calculated with $P_{0,0} = 0$ and $P_{0,0} = 0.04$ branching.

The *K*3 efficiency curves are free of inflection points. These curves were fit to polynomials to allow interpolation. Then, a least squares fitting approach was used, setting N_0 in Equation (1) as the only free parameter, to obtain the best fit of the experimental data to the *K*3 model. As shown by the reduced χ^2 values (Table 6), the fits were generally good with trending in the residuals varying for each model. Here, the difference in the activity determined with the DDEP- and Shearman-based branching schemes was >5 %, but the individual analyses gave no indication of a problem.

3.3. Emission intensities

The emission intensities (I_γ) measured with the S-detector for point sources and ampoules combined are listed in Table 7. The associated uncertainty budget for the 97.431 keV line is shown in Table 8. The measurement range for this detector is from 14 keV to 140 keV. Due to the low detection efficiency, weaker lines were not detected. The values obtained in this work are in agreement with the Shearman et al. (2017) values except for the 69.673 keV γ ray (difference of −6.6 %) and they are in disagreement with the DDEP calculated values (differences from −3.4 % to −5.4 %).

To obtain the I_γ for the weaker γ-ray lines, measurements were performed with the HPGe detectors, see Table 9 and Table 10. The differences between the S-detector and the HPGe detectors may be due to the detector response in the energy region of interest (Figs. S1–S3).

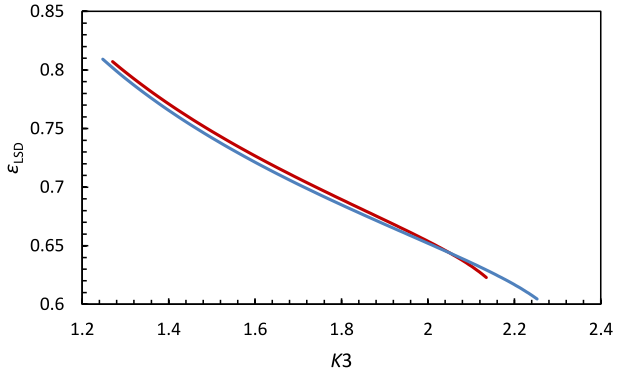

Fig. 9. Efficiency curves calculated according to the *K*3 model with $P_{0,0} = 0$ (blue) and $P_{0,0} = 0.04$ (red) branching.

Table 6
Fit results for the *K*3 model compared with the usual TDCR approach.

		kB	N_0	Reduced χ^2	Ratio
*K*3	Shearman	0.0075	1.820E+04	1.5E-06	1
		0.006	1.820E+04	3.7E-07	1.000
		0.009	1.781E+04	4.8E-06	0.979
	DDEP	0.0075	1.918E+04	5.1E-06	1.054
TDCR	Shearman	0.0075	1.804E+04		1
		0.006	2.175E+04		1.206
		0.009	1.795E+04		0.995
	DDEP	0.0075	1.781E+04		0.988

Table 7
Emission intensities measured using S-detector point sources and ampoules. Differences are relative to the NIST measured value. The uncertainty corresponds to one standard deviation.

Energy / keV	This work S-detector	Shearman et al. (2017)	DDEP (2020)DDEP (2020)
	I_γ	Difference / %	Difference / %
69.673	2.55 ± 0.04	−6.6	−5.0
97.431	30.02 ± 0.24	0.42	−3.4
103.18012	22.30 ± 0.20	0.15	−5.4

3.4. Half-lives

3.4.1. HPGe half-life

The half-life was determined based on the net peak area of the 97.4 keV γ ray measured by HPGe detector. The count rate was obtained from the net peak area fit and corrected by the decay of the source during the counting time (using the DDEP half-life value, 240.4(10) d) and the pile-up correction. These corrections to the count rates were smaller than 0.14 % and 0.02 % respectively and had no effect on the determined half-life to within the significant digits. The half-life was based on a weighted fit using smoothed uncertainties on the measured count rates; the residuals to the fit are shown in Fig. S4 and the full uncertainty budget, including high-, medium, and low-frequency components (Pommé, 2015; Pommé and De Hauwere, 2020; Pommé and Pelczar, 2021), is given in Table S2.

The ^{153}Gd half-life determined by HPGe spectrometry was $T_{1/2}$ = 238.19(97) d.

Table 8
Uncertainty budget for the 97.431 keV gamma-ray.

Uncertainty component	u_i / %
Full energy peak efficiency	0.30
Absolute activity	0.58
Geometry reproducibility	0.12
Peak Fitting	0.35
Decay correction	0.29
True coincidence summing	0.002
Combined standard uncertainty, u_c /%	0.80

Table 9
Emission intensities measured using X-detector point sources and ampoules. Differences are relative to the NIST measured value. The uncertainty corresponds to one standard deviation.

Energy /keV	This work X-detector	Shearman et al. (2017)	DDEP (2020)
	I_γ	Difference / %	Difference / %
69.673	2.49 ± 0.02	−4.41	−2.81
89.48595	0.096 ± 0.017	0.25	−4.26
97.431	30.29 ± 0.19	−0.47	−27.94
103.18012	22.46 ± 0.14	−0.56	−6.04
172.85307	0.041 ± 0.004	−2.27	−11.15

Table 10
Emission intensities measured using G-detector point sources and ampoules. Differences are relative to the NIST measured value. The uncertainty corresponds to one standard deviation.

Energy /keV	This work G-detector	Shearman et al. (2017)	DDEP (2020)
	I_γ	Difference / %	Difference / %
69.673	2.41 ± 0.07	−1.33	0.33
89.48595	0.078 ± 0.012	23.48	−11.25
97.431	30.00 ± 0.14	0.48	−3.35
103.18012	22.29 ± 0.11	0.18	−5.33
172.85307	0.043 ± 0.004	−7.06	−15.51

3.4.2. Vinten 671 ionization chamber

The half-life was calculated from a weighted least squares fit of the net currents measured on the Vinten 671 ionization chamber (VIC). Subsets of data from different time windows were analyzed to assess the sensitivity of the calculated half-life to periodic effects. The uncertainty on the half-life was calculated by combining this periodic variance with estimated uncertainties for background, source placement, and the fit to the data. Z-scores from the fit are given in Fig. S5 and the uncertainty budget is given in Table S3.

The ^{153}Gd half-life determined with the VIC was $T_{1/2} = 239.55(22)$ d.

3.4.3. Well-type NaI(Tl) detector

The half-life was determined based on weighted least squares fits of the count rates from an open window (15 keV to 2047 keV). Dry sources and solutions with 1 mol/L HCl and concentrated HCl were measured. It has been suggested by Kumar and Singh (1995) that the electron capture probabilities for ^{153}Gd are extremely sensitive to chemical environment, with K-capture probabilities for solid $GdCl_3$ being nearly 70 % higher than in concentrated acid environment. The significant changes to the decay mechanism suggested by Kumar and Singh would be expected to affect the ^{153}Gd decay constant.

Subsets of data from different time windows were analyzed to assess sensitivity to periodic effects. Periodic oscillations in the residuals (Fig. S6) were consistent for all sources and correlated with seasonal changes in ambient conditions (temperature and humidity). The seasonal oscillations were also observed in the net count rates for the ^{129}I check source. The standard deviation on the ^{129}I count rates, corrected for background, was used as an estimator for source placement uncertainty and a slight drift in the instrument response over the course of the measurements was included as a low-frequency source of uncertainty, as discussed by Pommé (2015). The combined standard uncertainty on the half-lives included contributions from the fit, time windows, linearity, drift, source positioning, and between-source variance.

The ^{153}Gd half-life determined with the NaI(Tl) well-type detector was $T_{1/2} = 239.34(25)$ d for the ampoules containing 1 mol/L HCl. The half-lives determined for the vials with 1 mol/L HCl, concentrated HCl, and dried material are given in Table 11. The half-lives determined for ^{153}Gd as dry $GdCl_3$ are consistent with those for ^{153}Gd in concentrated HCl to within the combined standard uncertainties.

Table 11
Half-lives determined using the NaI(Tl) well-type detector and sources prepared with ^{153}Gd in different chemical environments. Half-lives determined with other instruments are presented in the text.

Chemical environment	Vessel type	$T_{1/2}$(^{153}Gd) / d
1 mol/L HCl	ampoule	239.34(25)
1 mol/L HCl	vial	239.49(49)
Dry	vial	239.46(26)
concentrated HCl	vial	239.62(20)

4. Discussion

4.1. Rebalancing of decay scheme

The emission intensities for the 97.4 keV and the 103.2 keV γ ray agree with the recently published Shearman et al. (2017) values and disagree with the DDEP-evaluated values independent of the detector used to perform the measurements. Fig. 10A shows the emission intensity values for the 69.6 keV γ ray referenced in the DDEP evaluation displayed together with the value published by Shearman et al. (2017) and the currently measured values using the three different detectors. The emission intensities for the 103.2 keV γ ray and the 97.4 keV γ ray are shown in Fig. 10B and C.

As discussed, the new absolute emission intensities reported by Shearman et al. (2017) and herein necessitate a re-balancing of the ^{153}Gd decay scheme. This was done recently by Nica (2020), who noted that the available I_γ data are inconsistent. A very simple approach to re-balancing the decay scheme based on the Shearman et al. (2017) I_γ data was adopted here to estimate the impact on the electron capture branching for LS efficiency calculations. For γ-ray emissions not treated by Shearman et al. (2017) the DDEP (Bé et al., 2004) values for I_γ were used. Using conversion coefficients derived from DDEP, the gamma transition probabilities ($P_{\gamma+ce}$) were recalculated, allowing calculation of P_{ce} according to ($P_{ce} = P_{\gamma+ce} - I_\gamma$). The electron capture branching was then calculated by subtracting the sum of feeding transitions from the sum of transitions out of each level. The results of this approach are given in Table 12 and were renormalized for use in the LS efficiency models by setting the negative values to zero and adjusting the remaining weights to sum to 100 % ($P_{norm,i} = P_i / \sum P_i$). The rebalanced decay scheme is impacted principally by the updated $P_{\gamma+ce}$ for the 97.4 keV ($\gamma_{2,0}$) and 103.2 keV ($\gamma_{3,0}$) transitions. Table 12 also shows the results of the same rebalancing procedure using the values for I_γ determined with the S-detector (Table 7).

4.2. Impact of rebalanced decay scheme on measurements and between-method agreement

The LTAC-determined massic activity was the basis for the NIST contribution to the SIR (Michotte et al., 2021). As shown in Section 3.1, the LTAC experiment was designed to be robust against the choice of $P_{0,0}$. In LTAC, a correction for the differences in K/L capture between the different electron capture transitions would be required for the decay scheme with $P_{0,0} = 0.04$ since the γ-ray channel used to determine the LS efficiency is not sensitive to the γ-less $\epsilon_{0,0}$ decay (this is the "Funck correction"; Funck and Nylandstedt Larsen, 1983; Chauvenet et al., 1987; Fitzgerald et al., 2015). When $P_{0,0} = 0$, no such correction should be required. As the Geant4 simulations illustrate, the use of a weighted combination of gates obviates the need for a correction. Similarly, the digital coincidence counting experiment at NPL (Shearman et al., 2017) used a multi-dimensional extrapolation method, including gates set over the K x rays and the 97 keV and 103 keV γ rays. It is expected, and the agreement between NIST- and NPL-determined I_γs confirms, that the coincidence counting approaches at both labs are insensitive to $P_{0,0}$.

As discussed, a reasonable analysis of the TDCR data is only possible with a revised decay scheme with reduced weight for the $\epsilon_{0,0}$ transition.

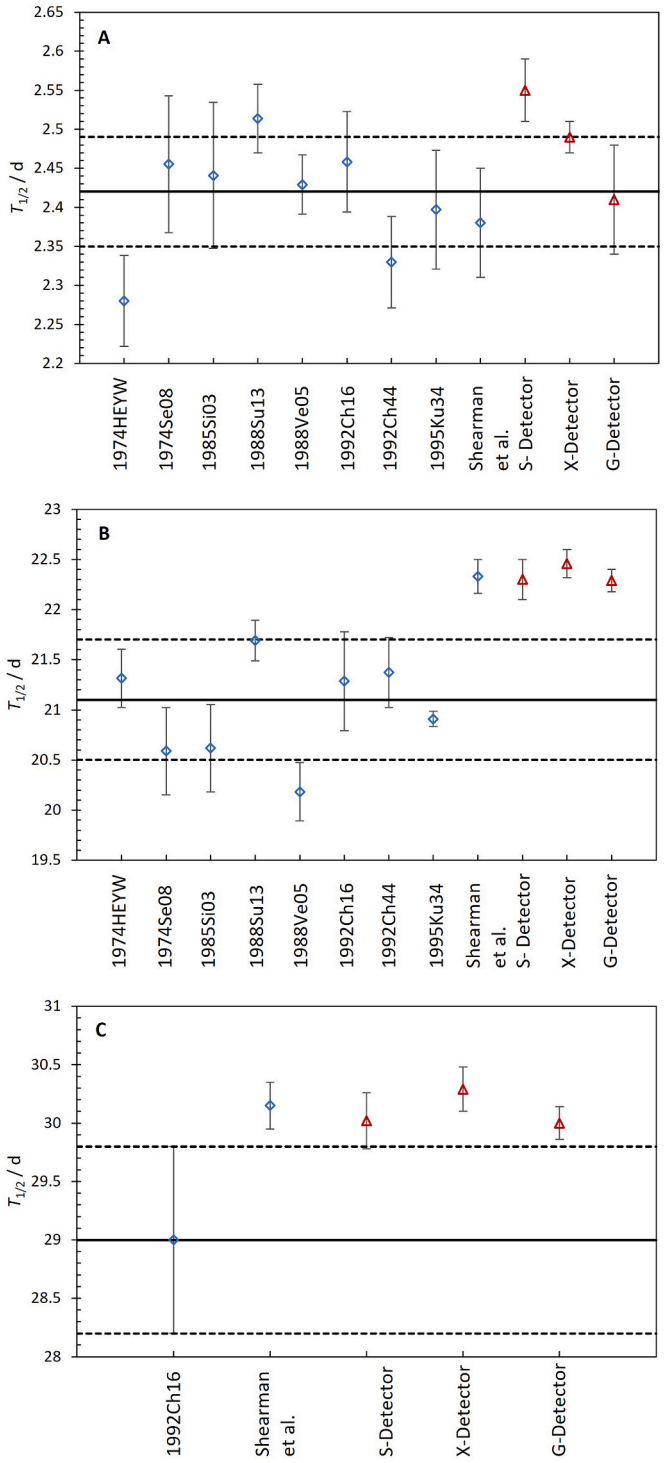

Fig. 10. Emission intensity values for (A) the 69.7 keV γ ray, (B) the 103.2 keV γ ray, and (C) the 97.4 keV γ ray referenced in the DDEP evaluation displayed together with the value published by Shearman et al. (2017) and the currently measured values using the three different detectors. The lines represent the DDEP evaluated values and their uncertainties.

With a scheme assuming $P_{0,0} = 0$, the 1.0 % relative combined standard uncertainty on the massic activity determined by TDCR counting is mostly due to the model uncertainty, estimated as the sensitivity to changing *kB* from 0.0075 cm MeV^{-1} to 0.009 cm MeV^{-1}. The TDCR massic activity is in accord with LTAC, with $A_{m,TDCR}/A_{m,LTAC} = 1.0027$ (58), where the stated uncertainty is the relative combined standard uncertainty from LTAC only. Agreement further improves when the stochastic asymmetry correction is used, giving $A_{m,TDCR}/A_{m,LTAC} = 0.9996(58)$.

Table 12
Electron capture branching calculated using I_γ values from Shearman et al. (2017) and the S-detector.

EC	Shearman	S-detector
0,4	15.55	16.63
0,3	45.54	44.41
0,2	39.40	39.24
0,1	−0.09	−0.09
0,0	−0.50	−0.27

From the LTAC activity, a calibration coefficient for the VIC was determined, $K_{VIC} = 1.180$ (9) pA MBq^{-1}, where the stated uncertainty is the combined standard uncertainty estimated from the uncertainty on the LTAC-determined activity, the measurement statistics, and the propagation of half-life, background, and weighing uncertainties. The uncertainty on the activity was the largest contributor to the combined standard uncertainty. Using the egs_chamber model of the VIC, values for K_{VIC} were estimated for [$P_{0,0} = 0.04$] and [$P_{0,0} = 0$] models. With $N = 5 \times 10^6$ decay events for each simulation, the model gave $K_{VIC} = 1.129$ (10) pA MBq^{-1} for $P_{0,0} = 0.04$ and $K_{VIC} = 1.150(11)$ pA MBq^{-1} for $P_{0,0} = 0$, where the stated uncertainties are from the Monte Carlo statistics only. While neither model gave satisfactory agreement with experiment, the [$P_{0,0} = 0$] decay scheme performs better.

Ionization chamber measurements on IC "A", with a *K*-value based on the 1998 NIST standardization, gave $A_{m,ICA}/A_{m,LTAC} = 1.0015(58)$, where the stated uncertainty is the LTAC uncertainty only. For the NIST AutoIC (Fitzgerald 2010), theoretical *K*-values based on benchmarked response curves were used to determine massic activities, finding $A_{m,AutoIC}/A_{m,LTAC} = 0.9699(58)$ with $P_{0,0} = 0.04$ and $A_{m,AutoIC}/A_{m,LTAC} = 1.0030(58)$ with $P_{0,0} = 0$.

Liquid scintillation and ionization chamber results alike show improved accord with LTAC when adopting a decay scheme with $P_{0,0} = 0$.

4.3. Half-life

The new NIST half-life determinations discussed herein all carry larger uncertainties than the Unterweger (1992) value ($T_{1/2} = 239.47(7)$ d) that is currently used in the DDEP evaluation (Bé et al., 2004). Since the DDEP evaluation, a problem with the ionization chamber source holder was discovered and the Unterweger value and its uncertainty were updated ($T_{1/2} = 239.29(10)$ d) to correct for the gradual change in source height (Unterweger and Fitzgerald, 2014, 2020). Even with the increased uncertainty estimated on the Unterweger value, it remains the most precise measurement of the ^{153}Gd half-life available. The new NIST measurements all carry larger uncertainties and therefore would not supplant the previous NIST half-life determination in a new evaluation. Using the Limitation of Relative Statistical Weights Method (Browne, 1998 and references therein), a new evaluation would be expected to give the same $T_{1/2}$ as the current DDEP evaluation, but with slightly increased uncertainty ($T_{1/2} = 240.4(10)$ d would become $T_{1/2} = 240.4$ (11) d). While the HPGe-determined half-life is discrepant, the remaining determinations described here (including ionization chamber- and NaI(Tl) well-type detector-determined values) are consistent with the Unterweger value. Fig. 11 shows the half-life values included in the DDEP evaluation, along with the revised Unterweger value and the new NIST measurements.

5. Conclusions

Questions surrounding the ^{153} Gd day scheme, raised in part by observed discrepancies with the SIRIC model, have been conclusively resolved by the work of Shearman et al. (2017) and the new

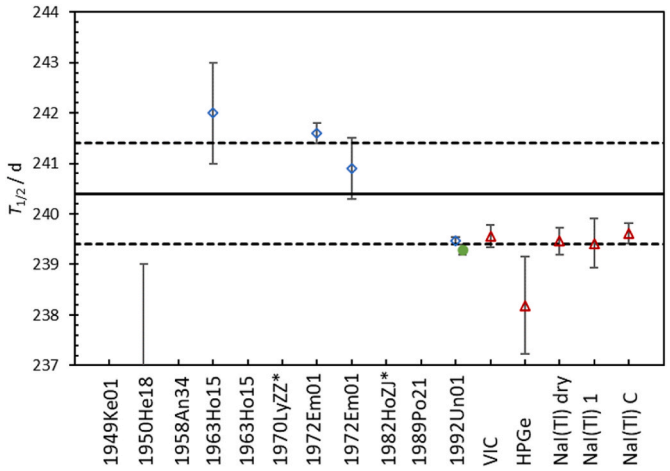

Fig. 11. Half-life values included in the DDEP evaluation (blue open diamonds), with the revised Unterweger value (green closed circle) and determinations from this study (red open triangles). NaI(Tl) well counter results include the different chemical environments summarized in Table 11: dry (labeled "dry"), 1 mol/L HCl (labeled "1"), and concentrated HCl (labeled "C"). Values that were superseded in the DDEP evaluation by subsequent measurements are indicated with an asterisk. Where no symbol is visible, the reported half-life value falls below the range shown. The black and dashed lines represent the DDEP half-life and its uncertainty.

measurements described herein. A decay scheme including 4 % direct electron capture decay to the ground state ($P_{0,0} = 0.04$) is inconsistent with experiment.

In this study, a ^{153}Gd solution was standardized for activity by live-timed anticoincidence counting with γ-gates optimized by Monte Carlo simulation to be insensitive to the choice of $P_{0,0}$. Absolute emission intensities for the main γ rays (I_γ) were determined by γ-ray spectrometry with HPGe and Si(Li) detectors. For the 97.4 keV and 103.2 keV γ rays, the present work is consistent with Shearman et al. (2017). For the 69.7 keV γ ray, the use of a Si(Li) detector, with a more linear efficiency curve at this energy, is discrepant with Shearman et al. (2017), giving a more reliable and precise value. The re-balancing of the ^{153}Gd decay scheme is principally informed by the I_γ for the 97.4 keV and 103.2 keV γ rays, so both the new measurements and the Shearman et al. (2017) measurements give consistent decay schemes—both with $P_{0,0} = 0$. Updated I_γ values will affect activity assays by γ-ray spectrometry as well as dosimetry calculations in nuclear medicine.

Efficiencies calculated for the triple-to-double coincidence (TDCR) method of liquid scintillation counting are very sensitive to electron capture branch weights. In this work, it was demonstrated that a model based on $P_{0,0} = 0$ provides a much better description of the experimental data and produces efficiencies very close to the empirical efficiencies calculated from the LTAC-determined massic activity. A stochastic asymmetry correction brought the TDCR results into excellent accord with LTAC. The CIEMAT-NIST efficiency tracing and K3 methods yield monotonic efficiency curves, making data analysis "easier", but potentially allowing hidden bias from an inappropriate efficiency model.

Several new half-life determinations were reported. The measurements were generally consistent with the revised Unterweger value (Unterweger and Fitzgerald, 2020), but with larger estimated uncertainties; as such, the new measurements would not impact the half-life in a new data evaluation. Half-life determinations with a NaI (Tl) well-type detector showed no difference between ^{153}Gd as dry $GdCl_3$ or in concentrated HCl, suggesting that the electron capture decay is not influenced by chemical environment to within the limits of detection in this experiment.

CRediT authorship contribution statement

Denis E. Bergeron: Writing – review & editing, Writing – original draft, Visualization, Methodology, Investigation, Formal analysis, Conceptualization. **Jeffrey T. Cessna:** Writing – review & editing, Methodology, Investigation, Conceptualization. **Ryan P. Fitzgerald:** Writing – review & editing, Writing – original draft, Methodology, Investigation, Formal analysis, Conceptualization. **Gulakhshan Hamad:** Writing – review & editing, Writing – original draft, Software, Methodology, Formal analysis. **Lizbeth Laureano-Pérez:** Writing – review & editing, Investigation, Formal analysis, Conceptualization. **Leticia Pibida:** Writing – review & editing, Writing – original draft, Methodology, Investigation, Formal analysis, Conceptualization. **Brian E. Zimmerman:** Writing – review & editing, Formal analysis, Conceptualization.

Declaration of competing interest

The authors declare that they have no known competing financial interests or personal relationships that could have appeared to influence the work reported in this paper.

Data availability

Data will be made available on request.

Acknowledgements

We are grateful to John Keightley, Sean Collins, and Rob Shearman (NPL) for fruitful collegial exchanges and to Stefaan Pommé (JRC), for providing software for empirical decomposition.

Appendix A. Supplementary data

Supplementary data to this article can be found online at https://doi.org/10.1016/j.apradiso.2023.111108.

References

Agostinelli, S., Allison, J., Amako, E., et al., 2003. GEANT4 – a simulation toolkit. Nucl. Instrum. Methods Phys. Res. 506, 250–303.
Amiot, M.N., Bé, M.M., Branger, T., Cassette, P., Lépy, M.C., Ménesguen, Y., Da Silva, I., 2012. Standardization of 64Cu using and improved decay scheme. Nucl. Instrum. Methods Phys. Res. A 684, 97–104.
Bergeron, D.E., Fitzgerald, R., 2018. Monte Carlo modelling of live-timed anticoincidence (LTAC) counting for Cu-64. Appl. Radiat. Isot. 134, 280–285.
Bé, M.M., Chisté, V., Dulieu, C., Browne, E., Chechev, V., Kuzmenko, N., Helmer, R., Nichols, A., Schönfeld, E., Dersch, R., 2004. Monographie BIPM-5. Vol.2, Table of Radionuclides (A = 151 to 242).
Bergeron, D.E., Cessna, J.T., Fitzgerald, R., Pibida, L., Zimmerman, B.E., 2018. Standardization of ^{64}Cu activity. Appl. Radiat. Isot. 139, 266–273.
Broda, R., 2003. A review of the triple-to-double coincidence ratio (TDCR) method for standardizing radionuclides. Appl. Radiat. Isot. 58, 585–594.
Broda, R., Péron, M.N., Cassette, P., Terlikowska, T., Hainos, D., 1998. Standardization of ^{139}Ce by liquid scintillation counting using the triple to double coincidence ratio method. Appl. Radiat. Isot. 49, 1035–1040.
Broder, B.A., Bergeron, D.E., Fitzgerald, R., Zimmerman, B.E., 2023. Comparison of calibration factors for Vinten ionization chaber simulated using four Monte Carlo methods. Appl. Radiat. Isot. 202, 111068.
Browne, E., 1998. Limitation of Relative Statistical Weights, A Method for Evaluating Discrepant Data. INDC(NDS) – 363, Appendix 1. International Atomic Energy Agency, Vienna.
Brun, R., Rademakers, F., 1997. Root – an object oriented data analysis framework. Nucl. Instrum. Methods Phys. Res. A 389, 81–86.
Case, J.A., 2015. Minimizing the radiation dose of CT attenuation correction while improving image quality: the case for innovation. J. Nucl. Cardiol. 23, 1080–1085.
Chauvenet, B., Bouchard, J., Vatin, R., 1987. Calculation of extrapolation curves in the 4πβ-γ coincidence method. Appl. Radiat. Isot. 38, 41–44.
Collé, R., 2019. Ampoules for radioactivity standard reference Materials™. NISTIR 8254. https://doi.org/10.6028/NIST.IR.8254.
Cox, M.G., Michotte, C., Pearce, A.K., 2007. Measurement modelling of the International Reference System (SIR) for gamma emitting radionuclides. Monographie BIPM 7.
DDEP. accessed 2020. http://www.lnhb.fr/nuclear-data/nuclear-data-table/.

Dutsov, C., Cassette, Ph, Sabot, B., Mitev, K., 2020. Evaluation of the accidental coincidence counting rates in TDCR counting. Nucl. Instrum. Methods Phys. Res. 977, 164292.
Enger, S.A., Fisher, D.R., Flynn, R.T., 2013. Gadolinium-153 as a brachytherapy isotope. Phys. Med. Biol. 58, 957–964.
Famulari, G., Urlich, T., Armstrong, A., Enger, S.H., 2017. Practical aspects of 153Gd as a radioactive source for use in brachytherapy. Appl. Radiat. Isot. 130, 131–139.
Famulari, G., Pater, P., Enger, S.A., 2018. Microdosimetric evaluation of current and alternative brachytherapy sources – a Getant4-DNA simulation study. Int. J. Radiat. Oncol. Biol. Phys. 100, 270–277.
Fitzgerald, R., Schultz, M.K., 2008. Liquid-scintillation-based anticoincidence counting of Co-60 and Pb-210. Appl. Radiat. Isot. 66, 937–940.
Fitzgerald, R., 2010. An automated ionization chamber for secondary radioactivity standards. Appl. Radiat. Isot. 68, 1507–1509.
Fitzgerald, R., Bailat, C., Bobin, C., Keightley, J.D., 2015. Uncertainties in 4πβ-γ coincidence counting. Metrologia 52, S86–S96.
Fitzgerald, R., 2016. Monte Carlo based approach to the LS-NaI 4πβ-γ anticoincidence extrapolation and uncertainty. Appl. Radiat. Isot. 109, 308–313.
Frey, E.C., Tsui, B.M.W., 1995. A comparison of Gd-153 and Co-57 as transmission sources for simultaneous TCT and Tl-201 SPECT. IEEE Trans. Nucl. Sci. 42, 1201–1206.
Funck, E., Nylandstedt Larsen, A., 1983. The influence from low energy x-rays and Auger electrons on 4πβ-γ coincidence measurements of electron-capture-decaying nuclides. Int. J. Appl. Radiat. Isot. 34, 565–569.
Helmer, R.G., 2006. Nuclear data sheets for A = 153. Nucl. Data Sheets 107, 507–788.
Kawrakow, I., Mainegra-Hing, D.W.O. Rogers E., Tessier, F., Townson, R.W., Walters, B. R.B., 2000. EGSnrc Toolkit for Monte Carlo Simulation of Ionizing Radiation Transport. https://doi.org/10.4224/40001303.
Kossert, K., Grau Carles, A., 2010. Improved metho for the calculation of the counting efficiency of electron-capture nuclides in liquid scintillation samples. Appl. Radiat. Isot. 68, 1482–1488.
Kossert, K., Cassette, Ph, Grau Carles, A., Jörg, G., Gostomski, C.L.V., Nähle, O., Wolf, Ch, 2014. Extension of the TDCR model to compute counting efficiencies for radionuclides with complex decay schemes. Appl. Radiat. Isot. 87, 242–248.
Kossert, K., Sabot, B., Cassette, Ph, Coulon, R., Liu, H., 2020. On the photomultiplier-tube asymmetry in TDCR systems. Appl. Radiat. Isot. 163, 109223.
Kumar, V., Singh, K.K., 1995. The decay of ^{153}Gd. J. Radioanal. Nucl. Chem. 189, 3–13.
Lucas, L.L., 2008. Calibration of the massic activity of a solution of Tc-99. Appl. Radiat. Isot. 49, 1061–1064.
Michotte, C., Pearce, A.K., Cox, M.G., Gostely, J.-J., 2006. An approach based on the SIR measurement model of determining the ionization chamber efficiency curves, and a study of ^{65}Zn and ^{201}Tl photon emission intensities. Appl. Radiat. Isot. 64, 1147–1155.
Michotte, C., Courte, S., Nonis, M., Coulon, R., Judge, S., Bergeron, D.E., Cessna, J.T., Fitzgerald, R.P., Laureano-Perez, L., Pibida, L., 2021. Update of the BIPM comparison BIPM.RI(II)-K1.Gd-153 of activity measurements of the radionuclide ^{153}Gd to include the 2020 result of the NIST (United States). Metrologia 58, 06027.
Moneta, L., 2010. https://root.cern.ch/root/html534/tutorials/fit/NumericalMinimization.C.html. September, 2022.
Nica, N., 2020. Nuclear data sheets for A=153. Nucl. Data Sheets 170, 1–498.
National Institute of Standards and Technology (NIST), 2015. Certificate, Standard Reference Material 4927G, Hydrogen-3 Radioactivity Standard. Gaithersburg, MD.
NNDC. accessed 2020. https://www.nndc.bnl.gov/ensdf/.
Perisinakis, K., Theocharopoulos, N., Karkavitsas, N., Damilakis, J., 2002. Patient Effective radiation dose and associated risk from transmission scans using 153Gd line sources in cardiac SPECT studies. Health Phys. 83, 66–74.
Pommé, S., 2015. The uncertainty of the half-life. Metrologia 52, S51.
Pommé, S., De Hauwere, T., 2020. Derivation of an uncertainty propagation factor for half-life determinations. Appl. Radiat. Isot. 158, 109046.
Pommé, S., Pelczar, K., 2021. Empirical decompositions and error propagation of medium-term instabilities in half-life determinations. Metrologia 58, 035012.
Shearman, R., Collins, S.M., Keightley, J.D., Pearce, A.K., Garnier, J., 2017. Absolute intensities of the γ-ray emissions originating from the electron capture decay of ^{153}Gd. EPJ Web Conf. 146, 10008.
Townson, R., Tessier, F., Galea, R., 2018. EGSnrc calculation of activity calibration factors for the Vinten ionization chamber. Appl. Radiat. Isot. 134, 100–104.
Unterweger, M.P., Fitzgerald, R., 2014. Update of NIST half-life results corrected for ionization chamber source-holder instability. Appl. Radiat. Isot. 87, 92–94.
Unterweger, M.P., Fitzgerald, R., 2020. Corrigendum to "Update of NIST half-life results corrected for ionization chamber source-holder instability". Appl. Radiat. Isot. 159, 108976 [Appl. Radiat. Isot. 87 (2014) 92-94.
Xiaolong, H., 2010. Evaluation the decay data of ^{153}Gd. Appl. Radiat. Isot. 68, 18–22.
Zimmerman, B.E., Collé, R., Cessna, J.T., 2004. Construction and implementation of the NIST triple-to-double coincidence ratio (TDCR) spectrometer. Appl. Radiat. Isot. 60, 433–438.